AIP | Physics of Plasmas
#1 JOURNAL IN 2014 GOOGLE SCHOLAR METRICS FOR THE PLASMA & FUSION CATEGORY

Kinetic theory of phase space plateaux in a non-thermal energetic particle distribution

F. Eriksson, R. M. Nyqvist, and M. K. Lilley

Citation: Physics of Plasmas **22**, 092126 (2015); doi: 10.1063/1.4931468
View online: http://dx.doi.org/10.1063/1.4931468
View Table of Contents: http://scitation.aip.org/content/aip/journal/pop/22/9?ver=pdfcov
Published by the AIP Publishing

Articles you may be interested in

Kinetic theory of the filamentation instability in a collisional current-driven plasma with nonextensive distribution
Phys. Plasmas **22**, 072103 (2015); 10.1063/1.4926521

Kinetic theory of nonlinear transport phenomena in complex plasmas
Phys. Plasmas **20**, 033701 (2013); 10.1063/1.4794968

Spectroscopic determination of kinetic parameters for frequency sweeping Alfvén eigenmodes
Phys. Plasmas **17**, 122311 (2010); 10.1063/1.3500224

Nonequilibrium electron distribution functions and nonlinear thermal transport
Phys. Plasmas **11**, 3997 (2004); 10.1063/1.1767832

Simulations and theories of relativistic ion cyclotron instabilities driven by MeV alpha particles in thermal deuterium plasmas
Phys. Plasmas **10**, 1315 (2003); 10.1063/1.1561611

TREK
www.trekinc.com

HIGH-VOLTAGE AMPLIFIERS AND ELECTROSTATIC VOLTMETERS
ENABLING RESEARCH AND INNOVATION IN DIELECTRICS, MICROFLUIDICS, MATERIALS, PLASMAS AND PIEZOS

This article is copyrighted as indicated in the article. Reuse of AIP content is subject to the terms at: http://scitation.aip.org/termsconditions. Downloaded to IP: 129.16.35.4 On: Mon, 05 Oct 2015 08:00:34

Kinetic theory of phase space plateaux in a non-thermal energetic particle distribution

F. Eriksson,[1,a)] R. M. Nyqvist,[1] and M. K. Lilley[2]
[1]Department of Earth and Space Sciences, Chalmers University of Technology, 41296 Göteborg, Sweden
[2]Physics Department, Imperial College, London SW7 2AZ, United Kingdom

(Received 11 March 2015; accepted 8 September 2015; published online 23 September 2015)

The transformation of kinetically unstable plasma eigenmodes into hole-clump pairs with temporally evolving carrier frequencies was recently attributed to the emergence of an intermediate stage in the mode evolution cycle, that of an unmodulated plateau in the phase space distribution of fast particles. The role of the plateau as the hole-clump breeding ground is further substantiated in this article via consideration of its linear and nonlinear stability in the presence of fast particle collisions and sources, which are known to affect the production rates and subsequent frequency sweeping of holes and clumps. In particular, collisional relaxation, as mediated by e.g. velocity space diffusion or even simple Krook-type collisions, is found to inhibit hole-clump generation and detachment from the plateau, as it should. On the other hand, slowing down of the fast particles turns out to have an asymmetrically destabilizing/stabilizing effect, which explains the well-known result that collisional drag enhances holes and their sweeping rates but suppresses clumps. It is further demonstrated that relaxation of the plateau edge gradients has only a minor quantitative effect and does not change the plateau stability qualitatively, unless the edge region extends far into the plateau shelf and the corresponding Landau pole needs to be taken into account. © *2015 AIP Publishing LLC*. [http://dx.doi.org/10.1063/1.4931468]

I. INTRODUCTION

Signals with rapidly shifting carrier frequencies are regularly observed in laboratory[1–6] and naturally occurring[7] plasmas. Extensive modelling has shown that their presence can be attributed to the formation and subsequent evolution of phase space *holes* and *clumps* in a non-thermal distribution of fast particles. The holes and clumps are nonlinear structures of Bernstein-Green-Kruskal (BGK) type[8] that extend in both momentum and real space, so named because they carry a particle deficit/surplus as compared to the surrounding particle distribution.[9–13] Disregarding the effects of fast particle collisions and sources, they arise symmetrically shifted off the wave-particle resonance of a kinetically unstable bulk plasma eigenmode. Once firmly established, they tend to balance dissipative wave damping in the background plasma with the energy tapped by traversing fast particle phase space as coherent entities. The resulting convective motion is synchronized to an evolution in the carrier frequencies of the corresponding signals, which gives rise to characteristic temporal sweeping patterns in the Fourier spectrograms.[14] When fast particle collisions and sources are taken into account, the nonlinear development of the eigenmode depends upon the type and rate thereof. Previous modelling has shown that whereas velocity space diffusion (e.g., pitch-angle scattering, energy diffusion, and scattering in radio frequency wave fields) and Krook-type collisions essentially act to inhibit hole-clump generation,[15,16] slowing down of the fast particles actually promotes, in particular, the formation of holes.[12,17]

The actual transformation of the unstable eigenmode into a hole-clump pair was recently attributed to the appearance of an intermediate stage in the mode evolution sequence, that of a plateau in the phase space distribution of fast particles and dissipative destabilization of negative-energy eigenmodes associated with that plateau.[18] However, the analysis of Ref. 18 was limited to the case of a collisionless energetic particle distribution, governed by the Vlasov rather than the Boltzmann equation, and moreover concerned only an idealized plateau velocity profile with a uniform interior and discontinuous jumps at the plateau edges. It is the purpose of the present article to further substantiate the plateau hypothesis for hole-clump production by extending the theory of Ref. 18 to include fast particle collisions and sources and account for more realistic, continuous plateau velocity profiles. Both steps are indeed necessary for the advancement of the plateau paradigm: As already mentioned, various types of fast particle collisions play decisive roles in the hole-clump formation process and, moreover, tend to relax the plateau edge gradient away from that of the discontinuous shelf model. However, plateaux with extended edge regions emerge in collisionless simulations too, especially when the unstable eigenmode is weakly driven close to its stability threshold.

The remainder of this article is organized as follows: Sec. II gives a brief introduction to the one-dimensional *bump-on-tail* model, which provides a simple framework for the description of hole-clump formation and will therefore be the consideration of this work. More detailed surveys on the logic behind such a simplification can be found elsewhere,[16,19] but the essential idea is that wave-particle interaction in an isolated resonance can be represented by a

a)frida.eriksson@chalmers.se

 © 2015 AIP Publishing LLC

This article is copyrighted as indicated in the article. Reuse of AIP content is subject to the terms at: http://scitation.aip.org/termsconditions. Downloaded to IP: 129.16.35.4 On: Mon, 05 Oct 2015 08:00:34

one-dimensional model.[20] Section III accounts for the occurrences of plateaux in various parameter regimes, far and marginally above the instability threshold and with and without fast particle collisions and sources. Then, in Secs. IV and V, nonlinear and linear calculations are presented, which attempt to explain the main features of Sec. III in terms of plateau stability theory. The focus of these sections is on the impact of deviations from the ideal plateau of Ref. 18 and the effects of fast particle collisions. Finally, Sec. VI summarizes the preceding sections and concludes the article.

II. MODEL EQUATIONS

We consider an electrostatic travelling wave with spatial period λ and wave number $k=2\pi/\lambda$ in a one-dimensional, uniform equilibrium plasma. The wave carrier frequency is assumed to be high enough that the plasma can be separated into a cold bulk, comprised of electrons and immobile ions, and a population of energetic electrons that may interact resonantly with the wave and therefore needs to be treated separately. Further, the perturbed electric field $E(x, t)$ is assumed to be small enough that the cold electron response is linear, and so their perturbed fluid velocity $V(x, t)$ satisfies the linearized fluid equation of motion

$$\frac{\partial V}{\partial t} = -\frac{e}{m}E - 2\gamma_d V. \tag{1}$$

Here, e and m are the (magnitude of the) charge and mass of the electron, respectively. The last term in Eq. (1) damps the velocity perturbation linearly (at a rate set by the parameter γ_d) and has been introduced in order to mock up various types of dissipative wave damping present in more realistic systems.[21–24]

The fast electrons are described kinetically in terms of a phase space distribution $F(x, v, t)$ that evolves according to the kinetic equation

$$\frac{\partial F}{\partial t} + v\frac{\partial F}{\partial x} - \frac{e}{m}E\frac{\partial F}{\partial v} = \mathfrak{C}[F] + S(v). \tag{2}$$

The right hand side of Eq. (2) represents fast particle collisions and sources, whose combined action is to relax F towards an equilibrium, or *unperturbed*, distribution $F_0(v)$ that, for simplicity, is taken as a constant, positive slope throughout the wave-particle resonance. They are modeled as the following combination of three operators, commonly known as Krook-type collisions, collisional drag, and velocity space diffusion

$$\mathfrak{C}[F] + S(v) = -\beta(F - F_0) + \frac{\alpha^2}{k}\frac{\partial}{\partial v}(F - F_0) + \frac{\nu^3}{k^2}\frac{\partial^2}{\partial v^2}(F - F_0). \tag{3}$$

The system of equations is closed by means of Ampére's law, which relates the perturbed currents in the two electron species to the electric field

$$\frac{\partial E}{\partial t} = \frac{e}{\epsilon_0}\left[n_0 V + \int v(F - F_0)dv\right]. \tag{4}$$

Here, n_0 is the unperturbed density of cold electrons (and immobile ions).

Assuming that the energetic electrons are of low density as compared to n_0, their perturbed current in Eq. (4) will be much smaller than that of the bulk electrons. If also the dissipation is assumed weak (in particular, if γ_d is significantly smaller than the wave carrier frequency), the perturbed electric field may be accurately represented as a single sinusoidal mode that oscillates at the electron plasma frequency $\omega_{pe} \equiv \sqrt{e^2 n_0/m\epsilon_0}$,

$$E(x, t) = A(t)\cos(kx - \omega_{pe}t), \tag{5}$$

and whose amplitude A evolves slowly in time as compared with the mode oscillations, $d\ln A/dt \ll \omega_{pe}$. The fast electrons are then most conveniently described in a frame that moves at the wave phase velocity ω_{pe}/k. All simulations in the present work are performed by means of a numerical algorithm, previously described in Ref. 12 and currently available online,[25] that, given a profile for F_0 and values for γ_d, β, α, and ν, solves Eqs. (1)–(4) for the nonlinear evolution of $E(x, t)$ and $F(x, v, t)$.

III. THE OCCURENCE OF PHASE SPACE PLATEAUX DURING HOLE-CLUMP FORMATION

The collisionless regime, with $\beta=\nu=\alpha=0$, was previously described in Ref. 18, but is discussed here in more detail. In the absence of dissipation, $\gamma_d=0$, the inverted slope of the unperturbed fast particle distribution F_0 causes wave growth due to phase mixing at linear rate $\gamma_L = (\pi\omega_{pe}^3/2k^2 n_0)dF_0/dv$. As the mode amplitude increases and the eye-shaped, flattened trapping region, bounded by the so called *separatrix* orbit, broadens its velocity width in phase space, the energy transfer from the fast particles gradually declines. It eventually ceases when the phase mixing can extract no more energy, at which point the wave amplitude has saturated at $\omega_B \equiv \sqrt{ekA/m} = 3.2\gamma_L$.[26] The saturation level is modulated, however, with sideband oscillations separated from ω_{pe} by roughly $0.4\gamma_L$.[12] Their presence is due to narrow, circulating bands, remnants from imperfect phase mixing on barely trapped orbits just inside the separatrix.

In the presence of dissipation, the linear growth rate alters to $\gamma_L - \gamma_d$. Far above the instability threshold, when $\gamma_d \ll \gamma_L$, the initial growth is then not very different from the dissipationless case. As the amplitude increases, the similarities wither, however, as shown in Fig. 1(a). Instead of saturating, the amplitude now reaches an initial peak value at which the energy transfer mediated by the phase mixing is balanced by the power dissipated in the bulk plasma. Beyond the maximum, the dissipation dominates and induces a decay on the longer time scale $1/\gamma_d$. The decline is oscillatory, however, again due to imperfect phase mixing on barely trapped orbits. As the amplitude decays, trapped particles gradually seep through the separatrix of the shrinking trapping region and begin to stream freely, which ultimately generates an almost completely rectangular, or *unmodulated*, phase space

This article is copyrighted as indicated in the article. Reuse of AIP content is subject to the terms at: http://scitation.aip.org/termsconditions. Downloaded to IP: 129.16.35.4 On: Mon, 05 Oct 2015 08:00:34

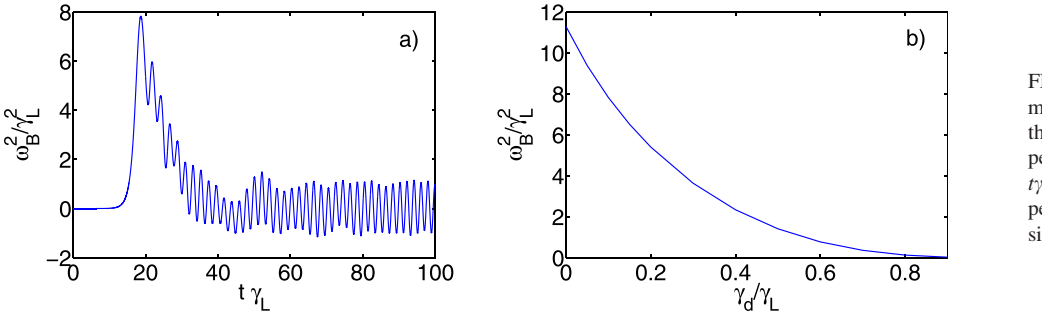

FIG. 1. (a) Temporal evolution of the mode amplitude when $\gamma_d/\gamma_L = 0.1$ in the collisionless limit. Note the initial peak value of $\omega_B^2/\gamma_L^2 \lesssim 8$ at around $t\gamma_L = 18$. (b) Amplitude at the initial peak as a function of γ_d/γ_L in the collisionless limit $\beta = \nu = \alpha = 0$.

plateau in the fast particle distribution, as portrayed in Ref. 18. The plateau is centered at the initial resonant velocity ω_{pe}/k and has a width slightly less than that of the separatrix at the amplitude maximum. At this stage, the initial mode is damped out and kinetically stable, but there are shifted resonances situated just inside the edges of the flat plateau region, responsible for a small modulation of the plateau edge, which begin to grow and eventually evolve into a hole-clump pair that detaches from the plateau.

The role of the plateau as a hole-clump breeding ground persists near the instability threshold too, although its build-up process is much more complex when the time scales of drive and damping are compared. Since the linear growth rate $\gamma_L - \gamma_d$ is small, it takes a longer time to reach the initial amplitude peak, but once there the high dissipation rate induces a much faster amplitude drop. As the dissipated power scales as $\gamma_d A^2$, the peak value is significantly lower marginally above than far from the threshold, as illustrated in Fig. 1(b). As a result, the emerging plateau is too small for the edge resonances to fully take off as holes and clumps. Instead we observe a series of false starts: The perturbations appear, form their separate trapping regions and attempt to detach, but instead trigger the bulk plasma mode, which phase mixes to a slightly larger amplitude peak than the previous. The ensuing dissipative damping generates a somewhat wider plateau, with growing edge resonances, and the entire process repeats until the plateau velocity width is large enough for hole-clump detachment to proceed, approximately $2\gamma_L/k$, as shown in Fig. 2(b). However, due to the complicated sequential build-up process the plateau edges are somewhat relaxed and its interior coarse-grained as compared to the smooth and distinct plateau that emerges far above the threshold. Unless otherwise specified, the remainder of this article focuses on the much simpler case $\gamma_d/\gamma_L = 0.1$.

Inclusion of fast particle collisions and sources, as described in Sec. II, has significant impact on the formation of holes and clumps. As previously mentioned in Sec. I, the Krook-type collision and velocity space diffusion operators both inhibit hole-clump production. The respective collision rates above which no holes and clumps develop are hard to pinpoint exactly given that there is a range of values throughout which they appear to form but then damp out. They lie at roughly $\beta/\gamma_L = 0.01$ and $\nu/\gamma_L = 0.1$, however, which are low enough values that the collisions do not significantly interfere with the initial stages that lead to the formation of the intermediate plateau state. Rather, the stabilization occurs due to the effect of the collisions on the plateau, as demonstrated in Figs. 3 and 4 in the case of

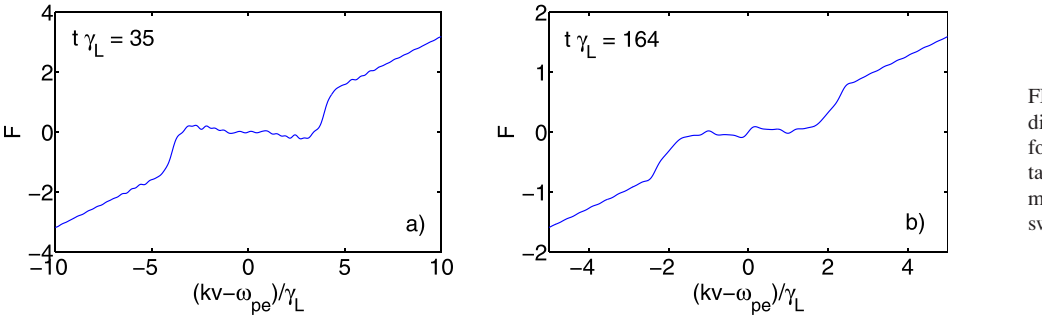

FIG. 2. Spatially averaged fast particle distribution in the collisionless limit for $\gamma_d/\gamma_L = 0.1$ (a) and $\gamma_d/\gamma_L = 0.9$ (b), taken just prior to the hole-clump formation and onset of frequency sweeping.

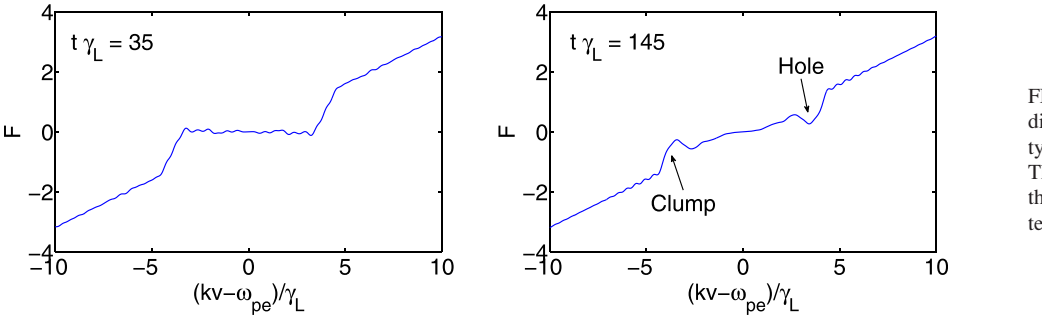

FIG. 3. Spatially averaged fast particle distribution in the presence of Krook-type collisions with rate $\beta/\gamma_L = 0.005$. The figures display a hole-clump pair that detaches from an intermediate plateau state.

This article is copyrighted as indicated in the article. Reuse of AIP content is subject to the terms at: http://scitation.aip.org/termsconditions. Downloaded to IP: 129.16.35.4 On: Mon, 05 Oct 2015 08:00:34

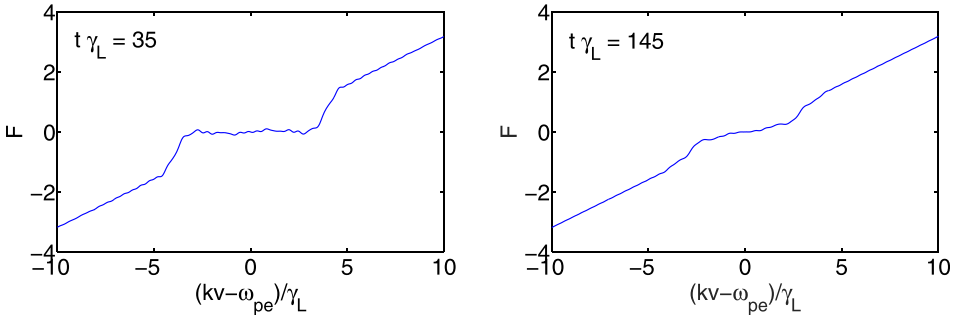

FIG. 4. Spatially averaged fast particle distribution in the presence of Krook-type collisions with rate $\beta/\gamma_L = 0.02$. The figures display the intermediate plateau stage, but no hole-clump generation.

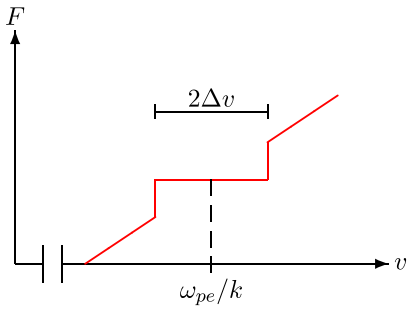

FIG. 5. Ideal shelf distribution with discontinuous edges.

Krook-type collisions. On the contrary, collisional drag turns out to promote hole-clump formation and detachment. The effect increases with the collision rate and is asymmetric in that holes develop at higher rates than clumps and become more pronounced perturbations in the fast particle distribution that take off faster with a more rapid frequency shift.

IV. STABILITY OF AN IDEAL PLATEAU

The aim of the present section is to substantiate the role of the intermediate plateau state via stability analysis of plateau distributions. We first show in Sec. IV A that large enough plateaux with discontinuous edges, cf. Fig. 5, support modes with phase velocities close to the shelf edges. The modes destabilize in the presence of dissipation and evolve nonlinearly into holes and clumps. We then demonstrate in Sec. IV B that relaxation of the discontinuous edge, via inclusion of a narrow transition region with a linear edge profile, plays a minor role for the plateau stability.

A. Shelf with discontinuous edges

The dispersion relation that governs the linear stability of the distribution in Fig. 5 was previously derived and analyzed in Ref. 18, but is discussed here in more detail and from a different perspective. It is given by

$$wz + i\pi\gamma = \log[1+z] - \log[1-z] - \frac{2z}{1-z^2}, \qquad (6)$$

where we have introduced the dimensionless variables

$$z \equiv \frac{\omega - \omega_{pe}}{k\Delta v}, \quad w \equiv \pi\frac{k\Delta v}{\gamma_L}, \quad \gamma \equiv \frac{\gamma_d}{\gamma_L}, \qquad (7)$$

log denotes the complex logarithm and it has been assumed that $|\mathrm{Re}[z]| < 1$, in which case the contribution from the Landau pole vanishes.

A numerical analysis reveals that Eq. (6) has precisely three complex roots with $|\mathrm{Re}[z]| < 1$ that depend on both w and γ. The solutions are most easily described when $\gamma = 0$. There is then always a root at $z = 0$, while the complementary two form a symmetric pair around $z = 0$ that is either purely real or imaginary, as shown in Fig. 6(a). The transition occurs at the *bifurcation width* $w_c(\gamma = 0) = 4$, beyond which the symmetric pair gradually tends towards the shelf edges at $z = \pm 1$ as w increases. The respective branches, henceforth denoted $z_\pm$, were dubbed *edge modes* in Ref. 18.

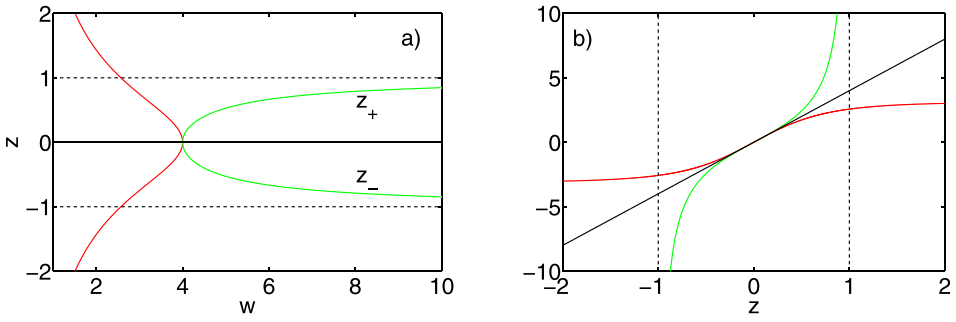

FIG. 6. (a) The three solutions of Eq. (6) when $\gamma = 0$. The black line is the mode at $z = 0$, while the green and red lines are the real ($z_\pm$) and imaginary branches, respectively. The dashed lines represent the shelf edges. (b) Graphical solution to Eq. (6) when $\gamma = 0$. The green and red lines are the right hand side of Eq. (6) for real and imaginary z, respectively. The black line is the left hand side when $w = w_c(0)$, at which all three lines osculate at $z = 0$ to generate a triple root. When $w > w_c(0)$, the black line intersects merely the green line (away from $z = 0$), which results in real solutions $z_\pm$, satisfying $-1 < z_- < 0 < z_+ < 1$. On the contrary, when $w < w_c(0)$ the black and red lines intersect, so the roots away from $z = 0$ are conjugated imaginary with diverging magnitudes as $w \to 0$. As in (a), the dashed lines represent the shelf edges.

This article is copyrighted as indicated in the article. Reuse of AIP content is subject to the terms at: http://scitation.aip.org/termsconditions. Downloaded to IP: 129.16.35.4 On: Mon, 05 Oct 2015 08:00:34

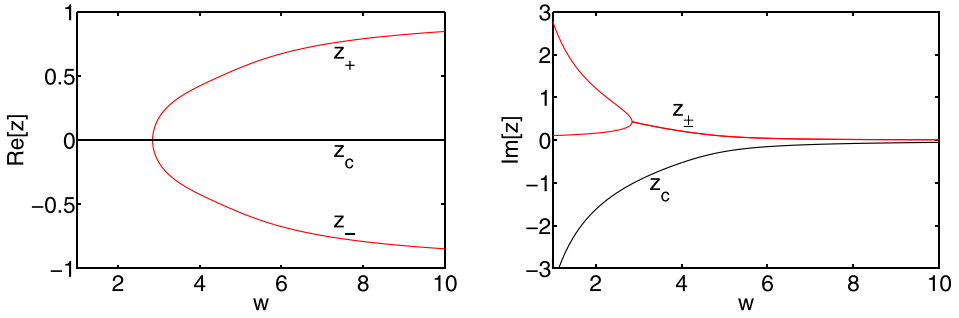

FIG. 7. Real (left) and imaginary (right) parts of the roots to Eq. (6) when $\gamma = 0.1$. The red lines are $z_\pm$ and the black lines are z_c.

Below the bifurcation width, the pair is conjugated imaginary and diverges symmetrically from $z = 0$ as w decreases. Nevertheless, the complex mode frequency $\omega = \omega_{pe} + k\Delta v z$ remains finite and the instability growth rate tends to γ_L as $w \to 0$, thus matching onto the plateau-less bump-on-tail instability, as it should. A supplementary, and standalone, graphical solution to Eq. (6) when $\gamma = 0$ is presented in Fig. 6(b) and its caption.

As shown in Fig. 7, finite dissipation, $\gamma > 0$, further distinguishes the solutions to Eq. (6) by separating the branches. It is found that whilst the mode at $z = 0$ remains at $\mathrm{Re}[z] = 0$ and is therefore dubbed the *central mode* and denoted z_c, it acquires a negative imaginary part that tends asymptotically to 0 as $w \to \infty$. The complementary two roots still share the branch $\mathrm{Re}[z] = 0$ with the central mode below the bifurcation, which now occurs at $w_c(\gamma) < w_c(\gamma = 0)$, as shown in Fig. 8(a), and split into a symmetric edge mode pair that asymptotes to $\mathrm{Re}[z_\pm] = \pm 1$ as $w \to \infty$. However, the edge modes get positive imaginary parts with finite γ, meaning that they are driven rather than damped by dissipation. Their imaginary parts are actually identical beyond $w_c(\gamma)$, eventually approaching 0 as $w \to \infty$, as seen in Fig. 7. The branches only separate below $w_c(\gamma)$, with one mode tending to $\mathrm{Im}[\omega] = \gamma_L - \gamma_d$ and the other to $\mathrm{Im}[\omega] = 0$ as $w \to 0$.

While it has been remarked that the shelf model should be used with caution[27] for damped modes, for which the dispersion relation can be shown to be discontinuous at the plateau edges if one relaxes the assumption $|\mathrm{Re}[z]| < 1$, the plateaux observed in the simulations all have w in the range $[2\pi, 4\pi]$ and so their central modes reside far from the shelf edges. All three modes of such plateaux are therefore fully consistent with the limitations imposed in Ref. 27, as previously noted.[28] Moreover, large w allows the roots to be accurately constructed as power series in $1/w$. To $\mathcal{O}(1/w^3)$, one obtains

$$z_\pm = \pm\left\{1 - \frac{1}{w}\left[1 + \frac{1}{w}(\ln 2w + 1/2) + \frac{1}{w^2}\left(\ln^2 2w + \ln 2w - 1/2 - \pi^2\gamma^2\right)\right]\right\} + i\frac{\pi\gamma}{w^2}\left[1 + \frac{1}{w}(2\ln 2w + 1)\right] \tag{8}$$

and

$$z_c = -i\frac{\pi\gamma}{w}\left[1 + \frac{4}{w} + \frac{16}{w^2}\left(1 - \frac{\pi^2\gamma^2}{6}\right)\right], \tag{9}$$

which are plotted and compared to the numerically obtained solutions in Fig. 8(b). Equation (8) clearly demonstrates that the edge modes are driven by dissipation, which strongly suggests that the modulations of the plateau edge that were found to develop into holes and clumps in Sec. III are, in fact, destabilized edge modes.

In order to verify that unstable edge modes evolve nonlinearly into detaching holes and clumps, the numerical algorithm of Sec. II is now set up with an initial plateau distribution for the fast particles,

$$F(x, v, t = 0) = C[v - \omega_{pe}/k][1 - R(v; \Delta v, a)]. \tag{10}$$

Here, $C = 2k^2 n_0 \gamma_L / \pi\omega_{pe}^3$ is the gradient of the ambient, linear slope that surrounds the plateau shelf and R is taken to be a smooth unit rectangle of the form

$$R(v; \Delta v, a) = \frac{1}{2}\sum_{\pm}(\pm 1)\tanh\left[\frac{v - \omega_{pe}/k \pm \Delta v}{a/k}\right], \tag{11}$$

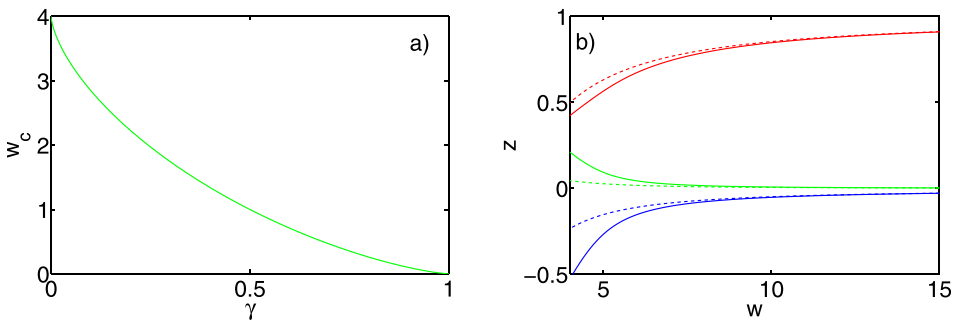

FIG. 8. (a) Dependence of w_c on γ for the discontinuous shelf model. Note that $w_c \to 0$ as $\gamma \to 1$, meaning that for $\gamma_d \geq \gamma_L$, the modes are always separate. (b) Numerically calculated roots ($\pm\,\mathrm{Re}[z_\pm]$ in red, $\mathrm{Im}[z_\pm]$ in green, and $\mathrm{Im}[z_c] = -iz_c$ in blue) and their approximations, Eqs. (8) and (9), dotted when $\gamma = 0.1$.

This article is copyrighted as indicated in the article. Reuse of AIP content is subject to the terms at: http://scitation.aip.org/termsconditions. Downloaded to IP: 129.16.35.4 On: Mon, 05 Oct 2015 08:00:34

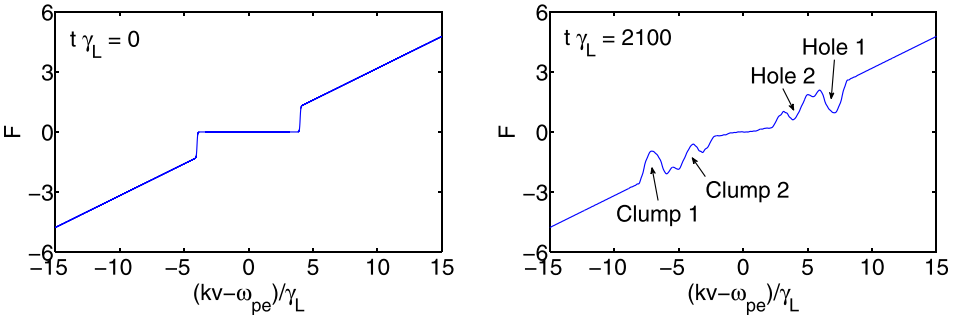

FIG. 9. Spatially averaged fast particle distribution as the initial shelf is evolved in the absence of fast particle collisions. The figure shows two detaching hole-clump pairs.

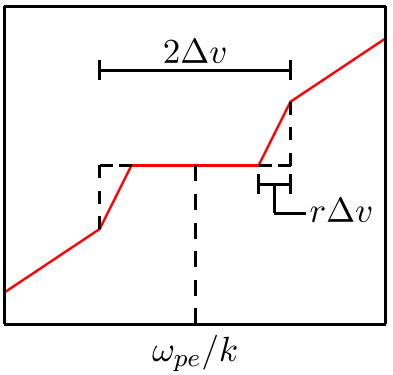

FIG. 10. A generalized shelf model with continuous edges.

meaning that a sets the extent of the edge region. In the limit $a \to 0$, this choice of initialization tends to the discontinuous distribution on display in Fig. 5, but the simulations must always be set up with finite a in order to minimize Gibbs's ripple phenomenon. Throughout the remainder of this article, unless otherwise specified, we take $a/\gamma_L = 0.05$ and $k\Delta v/\gamma_L = 4$ (which corresponds to $w = 4\pi$). The former is high enough to avoid ripples, but low enough that the plateau edges are approximately discontinuous, and the latter was chosen in order to replicate the plateaux observed in the simulations of Sec. III.

Fig. 9 indeed demonstrates how unstable edge modes develop into holes and clumps that take off from the initial plateau. When they do so, they peel off a portion of the plateau brim, in accordance with Liouville's theorem. The somewhat smaller shelf left behind is however still unstable, as shown in Fig. 9(b), where a secondary hole-clump pair has just detached and further reduced the plateau width.

B. Shelf with continuous edges

The plateaux observed in the simulations do not quite sport discontinuous edges, even though their edge gradients are large, cf. Figs. 2–4, so the question arises as to how sensitive the plateau hypothesis is to relaxation of the shelf edge gradients. We therefore generalize the model distribution in this section by including a narrow transition region that linearly joins the ambient distribution to the shelf level as in Fig. 10. Following the procedure outlined in Ref. 18, the dispersion relation becomes

$$wz + i\pi\gamma = \frac{r-1}{r}\big[\log[1+z] - \log[1-z]\big] + \frac{1}{r}\big[\log[1-r+z] - \log[1-r-z]\big], \qquad (12)$$

where r is defined in Fig. 10 and it has been assumed that $|\mathrm{Re}[z]| < 1 - r$. Note that Eq. (12) reduces to Eq. (6) in the limit $r \to 0$, as it should.

The solutions of Eq. (12) are very similar to that of the discontinuous shelf in Section IV A. There are once again three roots, of which one is a central mode with a negative imaginary part that vanishes at $\gamma = 0$ and whose magnitude increases with γ. It is supplemented by a symmetric pair that again bifurcates as w varies, but the bifurcation point and precise pattern now depend on r as well as γ, as shown in Fig. 11(a). The edge modes tend asymptotically to the edges of the flat region, at $\pm(1-r)$ rather than ± 1, as $w \to \infty$, and for a fixed w the modes shift with the edges towards the plateau center as r increases, as shown in Fig. 11(b). Their imaginary parts remain almost completely constant, however, meaning that relaxation of the shelf edge within a narrow transition layer has a negligible effect on the plateau stability. The latter conclusion is further supported by nonlinear simulations of an initial plateau state with $w = 4\pi$ and a-values ranging up to $0.1\gamma_L$, which corresponds to roughly $r = 0.1$. At larger a, however, the hole-clump production slows down and eventually terminates at $a/\gamma_L = 0.16$. The discrepancy is due to the contribution from the Landau pole

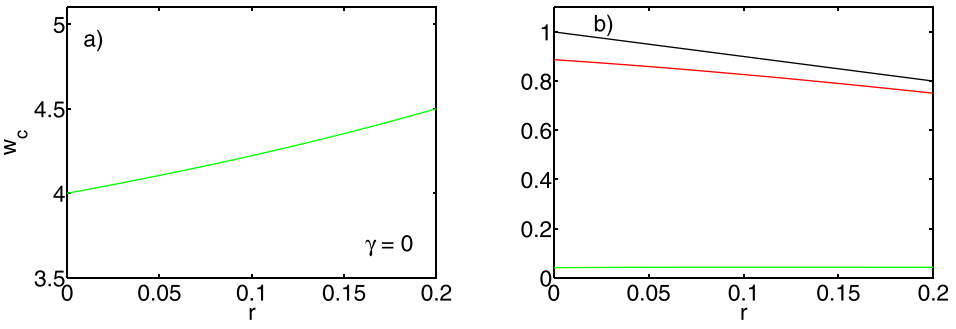

FIG. 11. (a) Dependence of w_c on r when $\gamma = 0$. (b) Edge modes, $\pm\,\mathrm{Re}[z_+]$ in red and $10 \times \mathrm{Im}[z_+]$ in green, as functions of r when $\gamma = 0.1$ and $w = 4\pi$. The black line represents the edge of the flat region, $1 - r$.

This article is copyrighted as indicated in the article. Reuse of AIP content is subject to the terms at: http://scitation.aip.org/termsconditions. Downloaded to IP: 129.16.35.4 On: Mon, 05 Oct 2015 08:00:34

associated with a non-negligible slope in the initial distribution of Eq. (10) at the edge mode resonances, which in fact reduces the edge mode growth rate.

V. EFFECT OF FAST PARTICLE COLLISIONS

We now proceed to further validate the plateau hypothesis by reconsidering the plateau stability problem in the presence of fast particle collisions and sources. Inclusion of the operators in Eq. (3) has essentially two effects. On the one hand, they act on perturbations from the plateau distribution, thereby affecting the growth rates (and possibly eigenfrequencies) of any instabilities. However, they also tend to relax the plateau as a whole towards the ambient, linear slope, which gradually changes the breeding ground for the modes and thereby their stability. The separation can be clearly visualized by means of Eq. (2), which after linearizing splits into two equations: An unmodulated part

$$\frac{\partial F_P}{\partial t} = -\beta(F_P - F_0) + \frac{\alpha^2}{k}\frac{\partial}{\partial v}(F_P - F_0) + \frac{\nu^3}{k^2}\frac{\partial^2}{\partial v^2}(F_P - F_0) \tag{13}$$

that governs the evolution of the spatially averaged ("plateau") distribution $F_P(v, t)$, and a modulated part

$$\frac{\partial \delta F}{\partial t} + v\frac{\partial \delta F}{\partial x} - \frac{e}{m}E\frac{\partial F_P}{\partial v} = -\beta\delta F + \frac{\alpha^2}{k}\frac{\partial \delta F}{\partial v} + \frac{\nu^3}{k^2}\frac{\partial^2 \delta F}{\partial v^2} \tag{14}$$

that determines the perturbation $\delta F(x, v, t) \equiv F(x, v, t) - F_P(v, t)$.

The linear problem turns out to be analytically tractable for both the Krook operator and collisional drag, in which case the procedure is to first solve Eq. (13) and plug the solution into Eq. (14), which then provides closure for Eqs. (1)–(4). One should note, however, that the time dependence of F_P leads to time dependent dispersion relations and mode frequencies that are only valid for $d\ln\omega/dt \ll \omega_{pe}$. The linear analysis is performed in Subsections V A and V B and compared with nonlinear simulations. The second order velocity space diffusion operator requires a numerical treatment, however, and is therefore analyzed exclusively nonlinearly.

A. Collisional relaxation

Starting with the Krook operator, the solution to Eq. (13) is simply an exponential decay of the initial distribution towards the linear slope F_0,

$$F_P(v, t) = F_0(v) + \mathrm{e}^{-\beta t}[F_P(v, t = 0) - F_0(v)]. \tag{15}$$

Taking, for simplicity, $F_P(v, t = 0)$ to be the discontinuous shelf in Fig. 5, the solution in Eq. (15) eventually leads to the dispersion relation

$$\begin{aligned} &w\mathrm{e}^{\beta t}z + i\pi\left[\gamma\mathrm{e}^{\beta t} - (\mathrm{e}^{\beta t} - 1)\right] \\ &\quad = \log[1 + (z + i\pi\beta/\gamma_L w)] - \log[1 - (z + i\pi\beta/\gamma_L w)] \\ &\qquad + \frac{1}{1 - (z + i\pi\beta/\gamma_L w)} - \frac{1}{1 + (z + i\pi\beta/\gamma_L w)}. \end{aligned} \tag{16}$$

The exponential functions on the left hand side are due to the collisional relaxation of the shelf interior. The presence of the Krook operator in Eq. (14), on the other hand, results in a shift of z of the terms on the right hand side of Eq. (16) by $i\pi\beta/\gamma_L w$.

Analyzing first the effect of the shift in the right hand side terms by setting $t = 0$, it is found that Krook collisions linearly damp the edge modes: For each pair of values for w and γ, there is a corresponding critical value of β, denoted β_c, above which the edge modes are initially linearly stable. For $\gamma = 0.1$, it ranges from $\beta_c/\gamma_L = 0.043$ at $w = 2\pi$ to $\beta_c/\gamma_L = 0.014$ at $w = 4\pi$, cf. Fig. 12(a). The latter shows good agreement with the results of Sec. III, which is actually a coincidence, as will be explained later on. In a similar fashion, the shift terms reduce the dissipative damping of the central mode, and there is another β-value above which the central mode is initially linearly unstable.

Turning now to the effect of the exponentials, it is found that the condition for initial linear stability is insufficient to predict the collision rate at which collisional termination of hole-clump generation from the plateau occurs. To begin with, the exponential multiplying w increases indefinitely, which gradually stabilizes the edge modes as time proceeds. A more important contribution, however, is the square bracket, which can be viewed as an effective dissipation rate that evolves as t advances and the plateau relaxes. For $\gamma \leq 1$, it decreases with time, eventually reaching negative numbers, which has a stabilizing effect on the edge modes. Consider a pair of initially linearly unstable edge modes, i.e. the case $\mathrm{Im}[\omega_\pm] > 0$ at $t = 0$. The time it takes to reach marginal stability as the plateau relaxes can be approximated by the instant at which the effective dissipation rate vanishes, $t_* = -\ln(1 - \gamma)/\beta$. Fig. 12(b) shows a plot of $\mathrm{Im}[\omega_\pm]t_*$ as function of β, which demonstrates that it is only below $\beta/\gamma_L \sim 0.0015$ that the edge modes increase their amplitude by an e-folding factor in the time t_* and therefore can be

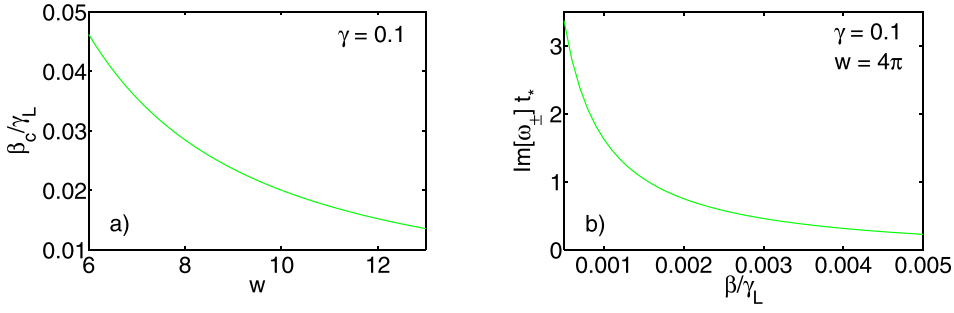

FIG. 12. (a) Rate of Krook collisions, β_c, above which the edge modes are linearly stable at $t = 0$, as a function of w when $\gamma = 0.1$. (b) $\mathrm{Im}[\omega_\pm]t_*$ as a function of β/γ_L when $w = 4\pi$ and $\gamma = 0.1$.

This article is copyrighted as indicated in the article. Reuse of AIP content is subject to the terms at: http://scitation.aip.org/termsconditions. Downloaded to IP: 129.16.35.4 On: Mon, 05 Oct 2015 08:00:34

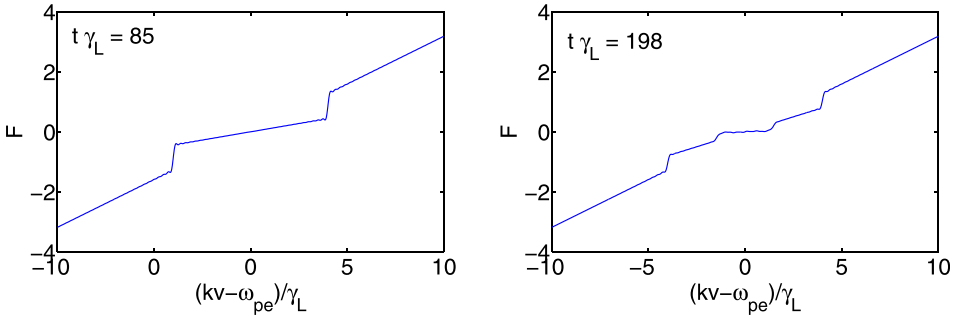

FIG. 13. Spatially averaged fast particle distribution as the initial shelf is evolved under the influence of Krook-type collisions acting at rate $\beta/\gamma_L = 0.005$. As shown, no hole-clump production occurs. Instead, the collisions gradually increase the gradient of the plateau interior until the central mode destabilizes and eventually establishes a secondary plateau (which is smaller than the initial one because the gradient required for excitation is less than the ambient slope, so there is less energy to be released by phase mixing).

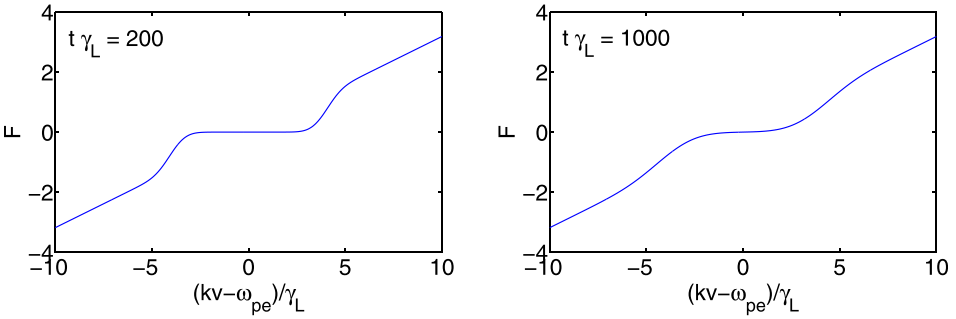

FIG. 14. Spatially averaged fast particle distribution as the initial shelf is evolved under the influence of velocity space diffusion with collision frequency $\nu/\gamma_L = 0.1$, at which hole-clump production is subdued. The collisions smear out the plateau edges diffusively, thereby relaxing the shelf towards the ambient, linear slope.

considered to survive into the nonlinear phase and evolve into holes and clumps. Accounting also for the fact that $\mathrm{Im}[\omega_\pm]$ actually decreases during the relaxation, a more reasonable estimate is that hole-clump production ceases somewhere in the range of $\beta/\gamma_L \lesssim 0.001$.

Nonlinear simulations confirm that Krook-type collisions indeed inhibit the formation of holes and clumps from an initial plateau, as demonstrated in Fig. 13, slightly below $\beta/\gamma_L = 0.001$, i.e. close to the rate predicted in Fig. 12(b) rather than β_c. The order of magnitude discrepancy with the simulations of Sec. III, where hole-clump production was found to cease around $\beta/\gamma_L = 0.01$, does, however, not depend on plateau-specific details, such as relaxation of the edge or non-flatness of the shelf interior. Rather, it stems from nonlinear excitation of the edge modes due to the presence of pre-existing sidebands already as the intermediate plateaux form.

In many aspects, the velocity space diffusion operator is very similar to that of Krook-type collisions. It inhibits hole-clump formation at around $\nu/\gamma_L = 0.05$ and it gradually drives the initial plateau distribution towards the ambient, linear slope. The relaxation proceeds diffusively, however, in contrast to the exponential action of the Krook operator. The effects are illustrated in Fig. 14, which portrays a simulation where the collision rate is high enough that no hole-clump pairs are created.

B. Slowing down of fast particles

In the presence of collisional drag, the solution to Eq. (13) is most easily obtained via an intermediate change of velocity variable to $u = kv + \alpha^2 t$, after which one finds that

$$F_P(v,t) = F_P(v + \alpha^2 t/k, t = 0) - C\alpha^2 t/k, \tag{17}$$

where again C is the slope of the ambient, linear distribution. The interpretation of Eq. (17) is that the drag operator simply convects the plateau down along the slope from the symmetrically centered position $v = \omega_{pe}/k$ at constant rate α^2/k. Inserting Eq. (17) into Eq. (14), and once more changing velocity variable as above, reveals that any perturbation from F_P merely slides along with the plateau. The dispersion relation then becomes that of a uniformly shifting plateau. Taking $F_P(v,\ t=0)$ to be the discontinuous distribution in Fig. 5, cf. Fig. 15, the dispersion relation becomes

$$wz + i\pi\gamma = \log[1 + s(t) + z] - \log[1 - s(t) - z] + \frac{1}{1 - s(t) - z} - \frac{1}{1 + s(t) + z}. \tag{18}$$

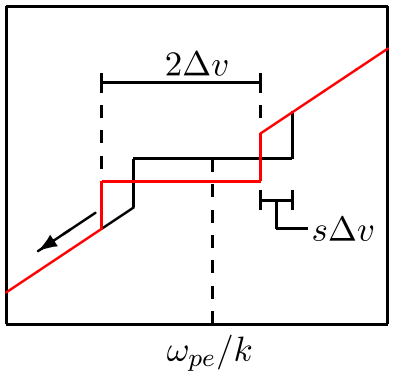

FIG. 15. Downshifting shelf with discontinuous edges.

This article is copyrighted as indicated in the article. Reuse of AIP content is subject to the terms at: http://scitation.aip.org/termsconditions. Downloaded to IP: 129.16.35.4 On: Mon, 05 Oct 2015 08:00:34

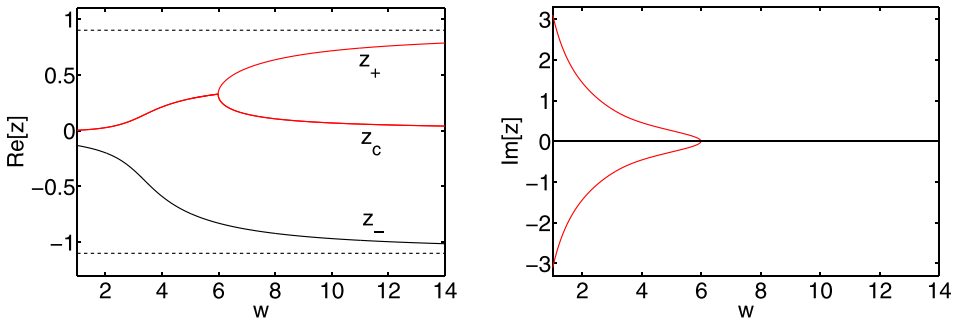

FIG. 16. Real (left) and imaginary (right) parts of the roots to Eq. (18) when $s = 0.1$ and $\gamma = 0$.

FIG. 17. Real (left) and imaginary (right) parts of the roots to Eq. (18) when $s = 0.1$ and $\gamma = 0.1$.

Here, $s(t) = (\alpha^2/k\Delta v)t$ and it has been assumed that $-(1+s) < \mathrm{Re}[z] < 1 - s$.

Inclusion of the plateau shift turns out to significantly alter the dependence of the roots on the plateau width w, in particular, for their real parts. First of all, even when $\gamma = 0$, as demonstrated in Fig. 16, all three modes are forced off the plasma frequency $\mathrm{Re}[z] = 0$. Below the bifurcation, which now occurs at $\mathrm{Re}[z] > 0$, the real parts of z_+ and z_c share a branch that tends to $\mathrm{Re}[z] = 0$ as $w \to 0$. The modes separate at the bifurcation width, after which the central mode tends to $z = 0$ and z_+ towards the upper shelf edge as $w \to \infty$. $\mathrm{Re}[z_-]$, on the other hand, shifts indefinitely towards the lower edge from -0.1 at $w = 0$. With finite γ, the bifurcation disappears altogether, cf. Fig. 17, so the modes are then truly separate. More importantly, non-vanishing s affects the growth rates of the edge modes unevenly when dissipation is present, as demonstrated in Fig. 17. This tendency can be seen analytically at order $1/w^2$ in the power series solution of Eq. (8) by taking s to be $\mathcal{O}(1/w)$, in which case

$$\mathrm{Im}[z_\pm] = \frac{\pi\gamma}{w^2}\left[1 + \frac{1}{w}(2\ln 2w + 1 \pm sw)\right]. \qquad (19)$$

As clearly demonstrated by the $\pm$ in front of the sw-term, the plateau model offers an explanation, in terms of linear stability, for the asymmetry between holes and clumps seen in the simulations. The results are further confirmed by nonlinear simulations, cf. Fig. 18.

VI. SUMMARY

The purpose of the present article has been to further attest the plateau hypothesis for hole-clump formation by extending the theory of Ref. 18 to account for fast particle collisions/sources and continuous plateau velocity profiles. Beyond giving an alternative and supplementary treatment of the idealized analysis in Ref. 18, two main findings are presented that both strengthen the conception of phase space plateaux as hole-clump breeding grounds: (1) Modest relaxation of the plateau edge gradient plays a minor role for hole-clump production. However, edge relaxation does become important when the gradient layer extends so far into the plateau shelf that the corresponding Landau pole cannot be neglected, in which case stabilization of the edge modes occurs. (2) The effects of fast particle collisions and sources conform to the results of current and previous simulations of

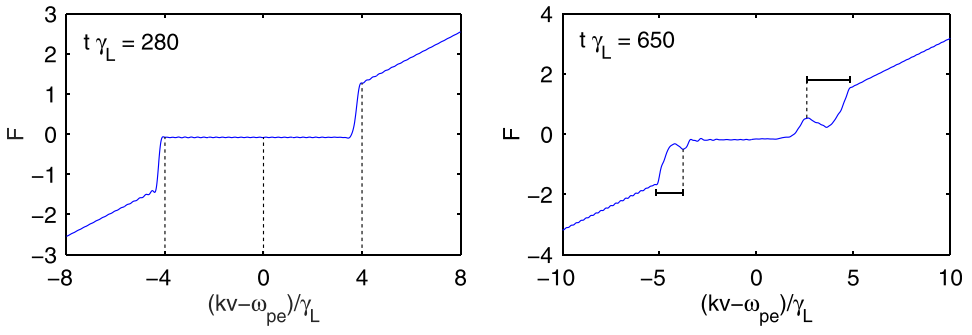

FIG. 18. Spatially averaged fast particle distribution as the initial shelf is evolved under the influence of collisional drag, acting at rate $\alpha/\gamma_L = 0.03$. Note the downward shift of the plateau on the left, visible albeit small, and that the hole on the right has almost twice the velocity width of the clump.

This article is copyrighted as indicated in the article. Reuse of AIP content is subject to the terms at: http://scitation.aip.org/termsconditions. Downloaded to IP: 129.16.35.4 On: Mon, 05 Oct 2015 08:00:34

a kinetically unstable plasma mode. Indeed, Krook-type collisions and velocity space diffusion are found to inhibit hole-clump production by reducing the edge mode growth rates, mainly via relaxation of the plateau rather than collisional damping of the modes. More interestingly, collisional drag generates an up-down asymmetry in the edge mode growth rates by convecting the entire plateau down along the slope in the ambient fast particle distribution, thereby explaining the previously observed preference of holes over clumps in the presence of fast particle drag. The presented results were found by means of a fully nonlinear numerical algorithm and confirmed by linear stability analysis.

The strong-drive focus of the present article, reflected in the generic choice $\gamma_d/\gamma_L = 0.1$, was adopted largely to separate the dissipative time scale from that of phase mixing in the initially unstable kinetic resonance, thereby simplifying considerably the discussion of the plateau formation stage and its subsequent stability. The authors are aware of the current consensus that excitation of Alfvénic modes tends to occur close to marginal stability. However, as already mentioned, one-dimensional simulations indicate that the role of the plateau as a hole-clump breeding ground persists when $0 < 1 - \gamma_d/\gamma_L \ll 1$. On the other hand, current observations of bursting toroidal Alfvén eigenmodes on the ASDEX Upgrade experiment suggest that kinetic mode excitation and hole-clump production may occur far above the instability threshold too,[29] which, in fact, lends experimental justification to the current study.

ACKNOWLEDGMENTS

The authors are grateful for inspiring discussions with Herb Berk that initially prompted the present work (and that presented in Ref. 18). We also highly appreciate enlightening discussions with Boris Breizman and the support given by Hans Nordman.

[1]D. Maslovsky, B. Levitt, and M. E. Mauel, Phys. Rev. Lett. **90**(18), 185001 (2003).
[2]E. Fredrickson, N. Gorelenkov, R. Bell, J. Menard, A. Roquemore, S. Kubota, N. Crocker, and W. Peebles, Nucl. Fusion **46**, 926 (2006).
[3]E. Fredrickson, R. E. Bell, D. S. Darrow, G. Y. Fu, and N. N. Gorelenkov, Phys. Plasmas **13**, 056109 (2006).
[4]M. P. Gryaznevich and S. E. Sharapov, Nucl. Fusion **46**, S942 (2006).
[5]H. L. Berk, C. J. Boswell, D. Borba, A. C. A. Figueiredo, T. Johnson, M. F. F. Nave, S. D. Pinches, S. E. Sharapov, and JET-EFDA Contributors, Nucl. Fusion **46**, S888 (2006).
[6]K. Shinohara, Y. Kusama, M. Takechi, A. Morioka, M. Ishikawa, N. Oyama, K. Tobita, T. Ozeki, S. Takeji, S. Moriyama, T. Fujita, T. Oikawa, T. Suzuki, T. Nishitani, T. Kondoh, S. Lee, M. Kuriyama, JT-60 Team, G. J. Kramer, N. N. Gorelenkov, R. Nazikian, C. Z. Cheng, G. Y. Fu, and A. Fukuyama, Nucl. Fusion **41**(5), 603 (2001).
[7]A. R. Soto-Chavez, G. Wang, A. Bhattacharjee, G. Y. Fu, and H. M. Smith, Geophys. Res. Lett. **41**, 1838, doi:10.1002/2014GL059320 (2014).
[8]I. B. Bernstein, J. M. Green, and M. D. Kruskal, Phys. Rev. **108**(3), 546 (1957).
[9]H. L. Berk, B. N. Breizman, and N. V. Petviashvili, Phys. Lett. A **234**, 213 (1997).
[10]R. G. L. Vann, H. L. Berk, and A. R. Soto-Chavez, Phys. Rev. Lett. **99**, 025003 (2007).
[11]M. Lesur, Y. Idomura, and X. Garbet, Phys. Plasmas **16**, 092305 (2009).
[12]M. K. Lilley, B. N. Breizman, and S. E. Sharapov, Phys. Plasmas **17**, 092305 (2010).
[13]S. D. Pinches, H. L. Berk, M. P. Gryaznevich, S. E. Sharapov, and JET-EFDA Contributors, Plasma Phys. Controlled Fusion **46**, S47 (2004).
[14]R. M. Nyqvist and B. N. Breizman, Phys. Plasmas **20**, 042106 (2013).
[15]H. L. Berk, B. N. Breizman, and M. Pekker, Phys. Rev. Lett. **76**(8), 1256 (1996).
[16]H. L. Berk, B. N. Breizman, J. Candy, M. Pekker, and N. V. Petviashvili, Phys. Plasmas **6**(8), 3102 (1999).
[17]M. K. Lilley, B. N. Breizman, and S. E. Sharapov, Phys. Rev. Lett. **102**, 195003 (2009).
[18]M. K. Lilley and R. M. Nyqvist, Phys. Rev. Lett. **112**, 155002 (2014).
[19]B. N. Breizman, H. L. Berk, M. S. Pekker, F. Porcelli, G. V. Stupakov, and K. L. Wong, Phys. Plasmas **4**(5), 1559 (1997).
[20]B. V. Chirikov, Phys. Rep. **52**, 263 (1979).
[21]R. Betti and J. P. Freidberg, Phys. Fluids B **4**(6), 1465 (1992).
[22]N. N. Gorelenkov and S. E. Sharapov, Phys. Scr. **45**, 163 (1992).
[23]M. N. Rosenbluth, H. L. Berk, J. W. Van Dam, and D. M. Lindberg, Phys. Rev. Lett. **68**(5), 596 (1992).
[24]R. M. Nyqvist and S. E. Sharapov, Phys. Plasmas **19**, 082517 (2012).
[25]M. K. Lilley (2010), source code available from https://github.com/mklilley/BOT.
[26]See National Technical Information Service Document No. AD730123 PGG-93, B. Fried, C. Lui, W. Means, and R. Sagdeev, University of California Report No. AD730123 PGG-93, 1971. Copies may be ordered from the National Technical Information Service, Springfield, Virginia 22161.
[27]I. Y. Dodin, Phys. Rev. Lett. **113**, 179501 (2014).
[28]M. K. Lilley and R. M. Nyqvist, Phys. Rev. Lett. **113**, 179502 (2014).
[29]P. Lauber, M. Schneller, X. Wang, A. Biancalani, D. Zarzoso, T. Hayward, G. Papp, B. D. Scott, S. D. Pinches, S. Sharapov, M. Maraschek, B. Geiger, V. Nikolaeva, L. Guimares, A. Mlynek, I. Classen, V. Igochine, A. Gude, and C. Hopf, in Theory of Fusion Plasmas: Joint Varenna-Lausanne International Workshop, Villa Monastero, Varenna, Italy, September 1–5, 2014.

This article is copyrighted as indicated in the article. Reuse of AIP content is subject to the terms at: http://scitation.aip.org/termsconditions. Downloaded to IP: 129.16.35.4 On: Mon, 05 Oct 2015 08:00:34